Tellus (2002), 54A, 338–349
Printed in UK. All rights reserved

TELLUS
ISSN 0280–6495

Saturation limiters for water vapour advection schemes: impact on orographic precipitation

By FRANCIS CODRON* and ROBERT SADOURNY, *Laboratoire de Météorologie Dynamique du CNRS, Paris, France*

(Manuscript received 10 November 2000; in final form 5 December 2001)

ABSTRACT

A common fault of atmospheric general circulation models (AGCMs) is an overestimation of orographic precipitation. One basic reason is that water vapour advection schemes do not use information about the local temperature. When water vapour is advected from a warm grid point to a colder one, supersaturation may occur on the way, and the water vapour advected may partly precipitate before reaching the latter. This process is particularly important when moisture is advected upward mountain slopes along terrain-following coordinates. Not taking it in account, i.e., letting all the moisture reach the colder point, leads to artificial drying of the windward valleys and foothills, and to overestimation of rainfall over summits and plateaux. This spurious behaviour is amplified by the resulting biases in the circulation, due to misplacement of the moisture convergence. It is a general bias, although its magnitude may be reduced, for instance when σ-coordinates are replaced by hybrid coordinates, or increased by highly diffusive schemes such as the upstream finite differencing. A simple way of correcting this bias is to test the advected water vapour with respect to saturation values, and redistribute it accordingly over the grid points found along the advecting path. This method is tested on a finite difference model using σ-coordinates and an upstream advection scheme. The effect on the distribution of moisture and rainfall is dramatic: precipitation is displaced from summits and plateaux to slopes and foothills, leading to much more realistic patterns, in particular for the Indian and Amazonian monsoons.

1. Introduction

In the past four decades, atmospheric general circulation models have improved slowly but constantly, progressing towards increasingly realistic simulations of atmosphere and climate. The significant increase in resolution allowed by the availability of increasingly powerful computers has played a large part in this evolution, especially for forecasting systems. In terms of resolution, climate models have always been lagging behind, due to the necessary trade-off between increasing the number of grid points and extending the length of simulations. In parallel to the increase in resolution, all facets of atmospheric dynamics have benefited from the improvements in modelling methods, both at the model scale (numerical methods) and at sub-grid scales (parameterisations). As a result, many systematic errors or climate drifts, i.e., drifts of numerical solutions with respect to analyses and observations, have been reduced. However, there are always remaining biases, and there is still ample scope for improving our models by scrutinising various physical processes.

In particular, those processes associated with the water cycle, such as convection, precipitation,

* Corresponding author. Present address: JISAO, Department of Atmospheric Sciences, University of Washington, Box 354 235, Seattle, WA 98195-4235, USA. e-mail: codron@atmos.washington.edu

or the formation of clouds, are still poorly modelled (Webb et al., 2001). The associated latent heating and radiative forcing are, however, an essential driving force of the atmospheric circulation. This dynamic response in turn influences the physical processes through the transport of moisture. This coupling means that a small inaccuracy can have large consequences on the modelled climate or its sensitivity.

The transport of moisture is itself difficult to simulate well: the transport scheme must represent the very heterogeneous distribution of water both in the horizontal and in the vertical, and at the same time avoid getting non-physical negative values or supersaturation, which would lead to spurious rainfall. The choice of advection scheme can thus have a significant impact on the simulated climate, as shown by Williamson and Rasch (1994) and Rasch and Williamson (1991) for zonal and global mean quantities, or by Nanjundiah (2000) for tropical rainfall. However, the advection scheme is not the only source of inaccuracies in the moisture transport.

For example, the errors associated with the near-cancellation of two large terms in the calculation of the horizontal pressure gradient in terrain-following coordinates have been to some extent alleviated by changing from the sigma coordinate of Phillips (1957) to more elaborate (hybrid) ones that are close to sigma near the ground but progressively tend to pressure or to potential temperature as one reaches the upper troposphere and the stratosphere (Simmons and Burridge, 1981; Zhu, 1997). However, even with such coordinates, the pressure gradient errors remain large near the ground along steep mountain slopes. One result is that spurious stationary spatial oscillations of the gravity wave type can be generated that unrealistically bring air flow over mountains even at low Froude numbers, when air masses are expected to flow around. The coupling of such oscillations with the water cycle leads to systematic errors, as computationally enhanced upslope winds artificially bring water vapour uphill and increase the probability of condensation there: the result is a computational increase of orographic precipitation, associated with artificial drying of the surrounding foothills or plains. Moreover, this effect is enhanced by the diffusion present in all water vapour advection schemes, even the less diffusive ones like those of Van Leer (1977) or Prather (1986), which produce an additional transport of water vapour uphill.

There is another systematic error associated with the transport of water vapour which, at least to our knowledge, has not been noticed hereto. In nature, condensation and precipitation are intimately linked to advection. The fact that numerical models treat the two processes separately and sequentially has some systematic consequences. Let us consider two neighbouring grid points P_u and P_d, P_u being upwind and P_d downwind. If P_d is significantly colder than P_u, then there is a strong probability that in nature the water vapour advected from P_u to P_d would condense and precipitate before reaching P_d. (In fact, there is even a strong probability that it would condense and precipitate close to P_u, because of the exponential dependence of the saturation mixing ratio on temperature.) In all advection schemes used so far, the advected water vapour is just added to the moisture already present at P_d. Thus, relatively large amounts of moisture can spuriously accumulate and eventually precipitate at cold grid points. Statistically, colder points being drier points, the result can be interpreted as additional artificial diffusion built into the water vapour advection scheme. This is a source of possibly large systematic errors, shifting moisture and precipitation patterns towards colder grid points.

A particular case where one can expect contrasted temperatures at grid points that are neighbours to each other is the case of steep mountain slopes in terrain-following coordinates. As mentioned above, there is already an artificial shift of the precipitation patterns towards the summits, due to the combined effect of horizontal pressure gradient errors, diffusive properties of the water vapour advection schemes and feedback between release of latent heat and low-level convergence. The systematic error due to the separation of condensation from water vapour advection will act as an additional bias enhancing the whole process and leading to even stronger spurious orographic precipitation. It is also likely to favour foothill drying, again because of the feedback between orographic convergence and latent heat release, and because of additional feedbacks associated with reevaporation of soil moisture.

This artificial separation between dynamical and physical processes also affects other variables, but the moisture content is particularly sensitive

because of its strong non-linear dependence on physical processes such as condensation.

The rest of the paper is organised as follows. Section 2 describes simple ways to modify water vapour advection and avoid this particular kind of systematic errors, in the case of finite difference models; our method uses flux limiters based on downstream saturation values. Section 3 describes the atmospheric model used for numerical experiments testing the impact of such systematic errors, and its sensitivity to our modifications of the water vapour advection scheme. The results on two paramount features of atmospheric general circulation and climate, the Asian and South American summer monsoons, are shown in Section 4. The impact we find is particularly strong, because our control experiment uses the first-order upstream advection scheme, which suffers from particularly strong numerical diffusion. A general discussion and some conclusions are given in Section 5.

2. Advection schemes

The conservation equation in flux form for the water vapour mixing ratio q reads:

$$\frac{\partial \rho q}{\partial t} + \mathrm{div}(\rho V q) = E - C \tag{1}$$

where ρ is the air density, V the velocity field, and E and C the evaporation and condensation rates. In a numerical model, the right-hand side of eq. (1) is computed by the model physics. The left-hand side can be integrated over the volume of a model grid box. The evolution of the water vapour content of the box is then equal to the sum of the inward fluxes through all its faces, the flux through one face $\delta Q/\delta t$ being:

$$\delta Q/\delta t = \rho V q^* \tag{2}$$

where q^* is the mixing ratio of the advected air.

The values of q are known at grid-point locations, not at the interfaces, q^* thus has to be computed. With global conservation ensured as soon as the same interface fluxes are used for the downstream and upstream boxes, the other properties of different advection schemes will depend on their estimate of q^*. The superscripts u and d will designate the values of variables at the points situated upstream and downstream relative to the wind, the subscript sat showing the saturation value. The simple and widely used 'first-order upstream scheme' uses $q^* = q^u$. It is positive and monotonic, but also very diffusive. More elaborate, less diffusive schemes, which calculate a subgrid distribution of q, were described for instance by Van Leer (1977) and Prather (1986).

There is, however, another constraint besides mass conservation that none of these schemes takes into account, which is that the water vapour should remain under saturation. To include this constraint, the temperature field, which determines the saturation mixing ratio value, must be considered. Figure 1 sketches the evolution of an air parcel advected from a warmer to a colder point, at which the saturation mixing ratio is lower than the initial mixing ratio of the parcel. The water vapour is conserved at first, until the parcel reaches saturation due to the decreasing temperature. The excess moisture then condenses, the parcel remaining at saturation while the mixing ratio goes down. The water vapour amount between points A and B in Fig. 1 will condense in the upstream box, while BC condenses over the downstream box. Using a first-order upstream scheme, all the moisture between A and C would be advected downstream and condense there. If the temperature profile is not too far from linear, the saturation curve has an exponential shape. AB is then much greater than BC, resulting in a large

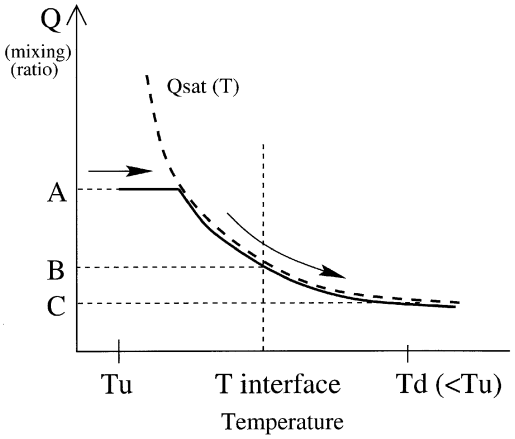

Fig. 1. Scheme of the evolution of the mixing ratio (continuous line) of a particle advected from a point at temperature T_u to a colder point T_d. The dashed line is the saturation mixing ratio.

error. The same problem, but with opposite sign (evaporation), can occur when liquid water is advected towards a warmer point. In this case, however, the error is much smaller, still because of the exponential shape of q_{sat}.

The sequential treatment of advection and condensation cannot be suppressed without changing the whole structure of GCMs. However, we can try to alter the distribution of water vapour resulting from the dynamics, so that condensation will take place at the right point (i.e., upstream of colder points). A simple solution is to impose an upper boundary $q^{\max}$ on the mixing ratio of the water vapour advected across the interface between two grid points. The water vapour flux becomes:

$$\delta Q/\delta t = \rho V \min(q^*, q^{\max}). \tag{3}$$

The water vapour above $q^{\max}$ which is not advected remains upstream, where it may eventually condense and precipitate.

The saturation mixing ratio at the interface $q^{\max} = q_{\mathrm{sat}}^{(T^{\mathrm{u}} + T^{\mathrm{d}})/2}$ seems a natural value for this upper bound (assuming a linear temperature profile). In the rest of this article, we use $q^{\max} = q_{\mathrm{sat}}^{\mathrm{d}}$, which is only a slightly lower value (due to the exponential shape of q_{sat}) and is easier to compute.

Using a lower value for $q^{\max}$ also incorporates the effects of the sub-grid scale heterogeneities of the water vapour distribution, which are parameterised in every general circulation model, and will cause condensation to begin before the averaged mixing ratio reaches saturation. A more elaborate scheme could use a smoother transition from q^* to $q^{\max}$ using a parameterisation of moisture sub-grid distribution, but we concentrate here on first-order effects.

Note that precipitation over the colder downstream point is not suppressed: large-scale condensation can occur with a moisture concentration under saturation because of sub-grid scale inhomogeneities, and convective precipitation does not need large-scale saturation.

2.1. *Semi-Lagrangian schemes*

A number of models use a semi-Lagrangian advection scheme, which enables using a longer time step with increased horizontal resolution. Using these schemes, water vapour can be advected over more than one grid point in a single time step. The problem we outlined then becomes even more critical, as for example moisture can be advected across a mountain range, suppressing the shadow effect.

Without going into technical details, the same solution could be applied: it would imply following air parcels from their origin point, and testing their mixing ratio against the saturation one each time their advection path crosses a grid-point boundary.

3. Model description

Sensitivity experiments were performed with Version 5b of the Atmospheric General Circulation Model (AGCM) of the Laboratoire de Météorologie Dynamique (LMD). It is a grid-point finite-difference model, identical to that described by Harzallah and Sadourny (1995), except for the surface drag coefficient. Condensation associated with non-convective processes is handled by a statistical scheme that allows condensation to occur before saturation is reached on a large scale. A uniform probability density function is used to describe the sub-grid variability of the total water within the grid box (Le Treut and Li, 1991). The half-width of the distribution is taken to be proportional to the total amount of water within the grid box.

A mean orography is used. The horizontal resolution is rather coarse: 64 points in longitude, and 50 points equally spaced in sine of latitude. The model uses terrain-following σ-coordinates in the vertical. Its other main features are summarised in Table 1.

The AGCM was forced by climatological SSTs, except in the tropical Pacific Ocean, where it was coupled with an oceanic GCM. The coupled climate is stable and quite realistic, and the effects of coupling on the sensitivity of precipitation to the advection schemes can be neglected in the regions considered in this study. The mean state, seasonal cycle and interannual variability in the tropical Pacific Ocean region are described by Vintzileos et al. (1999a,b).

The control run Ctrl is a 30-year integration in which a first-order upstream advection scheme is used, $q^* = q^{\mathrm{u}}$ using the notations of Section 2. The sensitivity experiment Qsat also lasts 30 years and uses the simple limiter $q^{\max} = q_{\mathrm{sat}}^{\mathrm{d}}$. The Qsat − Ctrl

Table 1. *LMD AGCM characteristics*

Horizontal resolution	64 longitude × 50 sine of latitude
Horizontal advection	Upstream acheme
Dynamic equations	Sadourny (1975)
Lateral diffusion	Bi-Laplacian
Vertical coordinate	11 layers in $\sigma = p/p_s$
Thermodynamic variable	Potential enthalpy $H = C_p T(p_s/p)^\kappa$
Short-wave radiation	Fouquart and Bonnel (1980)
Long-wave radiation	Morcrette (1991)
Cloud parameterisation	Le Treut and Li (1991)
Boundary layer	Bulk aerodynamic
Convection schemes	Manabe and Strickler (1964) saturated case Kuo (1965) unsaturated case

differences are stable from year to year, and their structure is different from the main modes of interannual variability. In fact, the results shown are significant above 99% according to a *t*-test.

The experiments with a higher ($96 \times 72 \times 19$) resolution were performed with a more recent version of the LMD GCM called LMDZ. The main differences from LMD5b are a cleaner writing of the dynamics which allows the possibility of a variable resolution (not used here), and the use of a regular grid in latitude. The parameterisations are unchanged, and the values of the parameters used were tuned one by one so that LMDZ has the same behaviour as the former versions. We chose for these experiments to keep the first-order upstream scheme and σ-coordinates, in order to be consistent with lower resolution experiments, and to maximise the sensitivity to the advection scheme change. These runs are both 5 years long.

4. Simulated precipitation sensitivity

The temperature difference between neighbouring grid points is most of the time small enough that the problem we consider here has only a weak effect on the simulated climate. Some small but significant influence can be observed in nearly saturated areas, such as the western Pacific warm pool. However, the main exception is near orography, where the advection along topography-following σ-surfaces can encounter steep temperature gradients due to their vertical component. As discussed in the introduction, moisture advection that is too strong also acts to enhance the effect of spurious air convergence over mountains forced by pressure gradient errors along these σ-surfaces.

Our analysis is thus focused on two regions where the orography plays an important role: the northern hemisphere Eurasian monsoon region during boreal summer, and South America during austral summer. In both cases, orographic influences are prominent on the precipitation patterns due to the Himalayas, the Tibetan Plateau and Central Africa mountains on the one hand, and to the Andes on the other hand.

4.1. Rainfall changes

The observations of Legates and Willmott (1990) of summer precipitation over South America are shown in Fig. 2, together with the results of the Ctrl and Qsat runs. The Qsat − Ctrl difference is shown with the model orography to see the location of changes more clearly.

The observed field (Fig. 2a) consists of a broad pattern covering Amazonia and the Brazilian plateau. In the Ctrl run (Fig. 2b) there are three distinct precipitation maxima over the Brazilian plateau, Ecuador and the Andes between 15°S and 25°S, the other areas being generally too dry.

The Ecuador and Brazil maxima are reduced in the Qsat run (Figs. 2c and d). Over the Andes, the heavy precipitation centre moves upwind in Qsat, and most of the rain falls on the north-eastern slopes instead of on the summit in Ctrl. It is better positioned when compared to the observations, and the almost desert dry band between 10°S and 15°S seen in Ctrl is suppressed. This unrealistic feature was the result of the subsiding branch of a local circulation cell driven by the strong latent heating over the summits.

The effect of the change of scheme is similar in the Asian monsoon simulation (Fig. 3). The very high orographic precipitation maxima simulated in Ctrl over Ethiopia and the Sumatra, Borneo and New Guinea Islands are reduced in Qsat to values closer to the observed ones. In Asia, the rainfall amount decreases over the Tibetan Plateau, and the main centre shifts north-westward from the centre of Burma to the Bay of Bengal. The wet tongue extending over the southern Himalaya foothills is better defined in Qsat. The

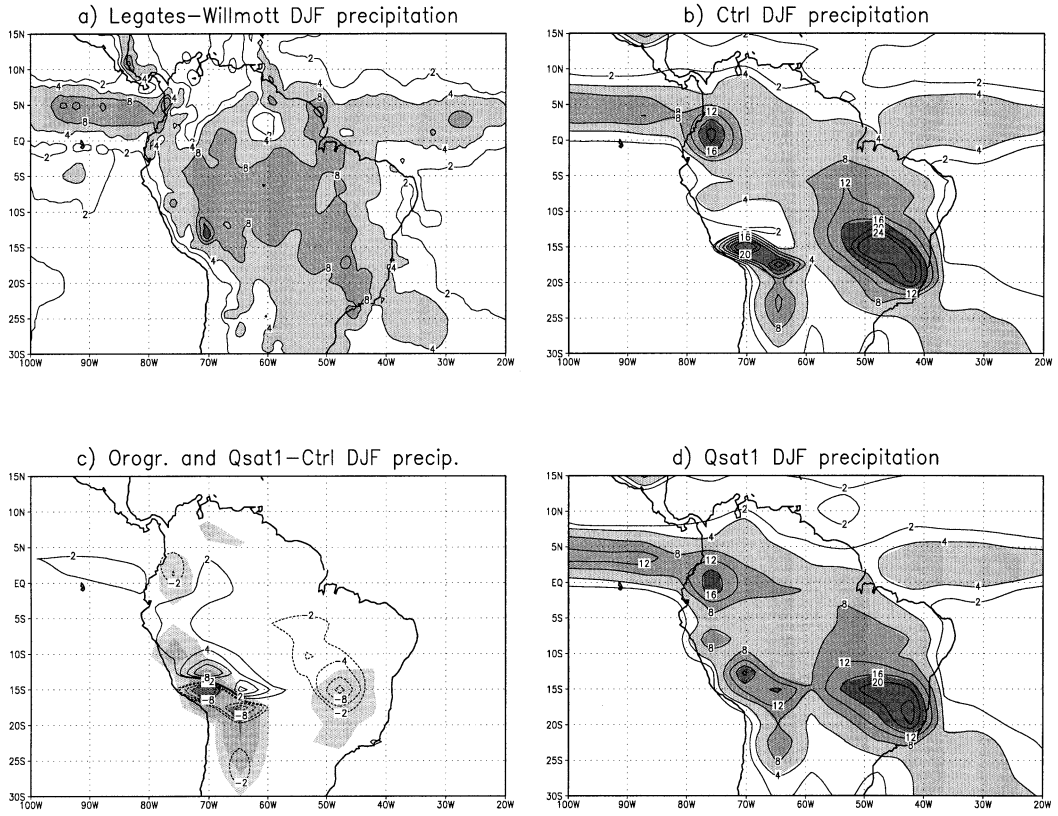

Fig. 2. December–January–February precipitation over South America (mm d^{-1}). (a) Climatology of Legates and Willmott (1990); (b and d) simulated by the Crtl (b) and Qsat (d) runs. The contours are every 4 and at 2 mm d^{-1}, shading is over 4, 8, and 16 mm d^{-1}. (c) Qsat – Ctrl difference (contours every 2 mm d^{-1}) and model topography (shading above 500, 1000 and 2000 m altitude).

Qsat simulation is thus generally more realistic, although some features, such as the Western Ghats barrier, are missing.

4.2. *Relative humidity*

To understand better the cause of the precipitation changes, Fig. 4 displays the relative humidity Q_{rel} at 5 m height in the Ctrl and Qsat runs over South America, as well as the Qsat – Ctrl difference.

In the Ctrl run, the relative humidity is above 90% over the areas of maximum precipitation, but much lower elsewhere. In the Qsat run, Q_{rel} is still high over mountain tops, but is much more spatially homogeneous. The Qsat – Ctrl differences indeed show that there is almost no decrease in Q_{rel} over Ecuador and the Brazilian plateau, where it remains just under saturation (Note that Q_{rel} is saved just after the physics package in the model, so it cannot in practice be supersaturated. However, a higher mixing ratio before the large-scale condensation is computed will still yield a higher mixing ratio after condensation.) The precipitation decreases in these areas because in Qsat, Q_{rel} does not get over saturation before condensation occurs.

There is, however, a large increase in relative humidity in Qsat in the dry area simulated in Ctrl on the northern slopes and foothills of the Andes. The moisture brought by the easterly winds (Fig. 4c) remains in the valleys and on the slopes instead of being advected to the summits, and can accumulate then precipitate there.

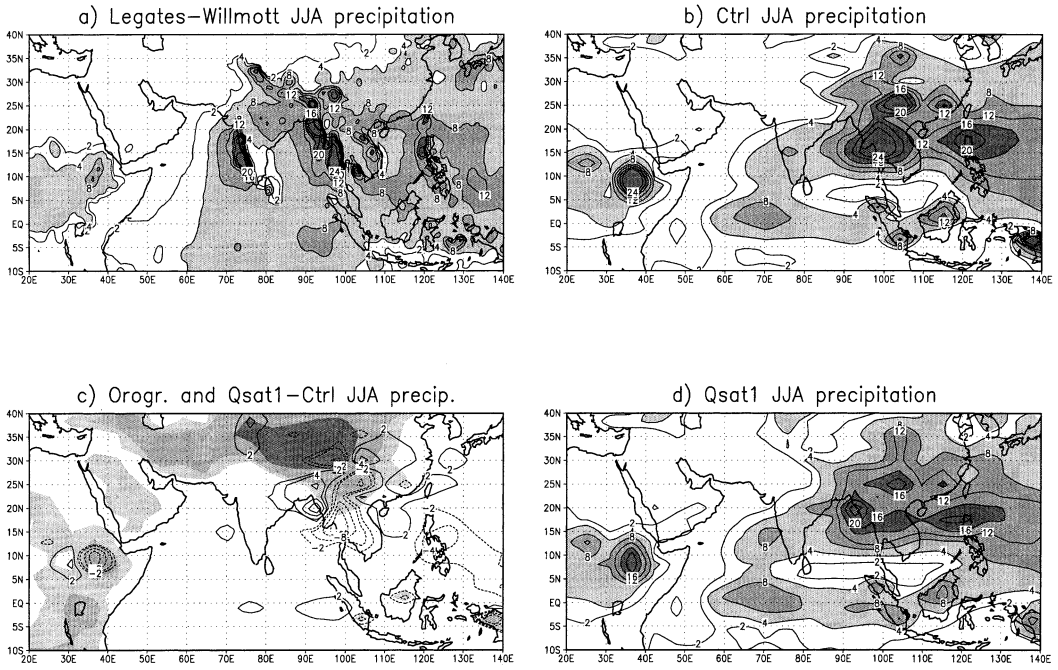

Fig. 3. June–July–August monsoon precipitation (mm d^{-1}). (a) Climatology of Legates and Willmott (1990); (b and d) simulated with advection schemes Ctrl (b) and Qsat (d). Contours are every 4 and at 2 mm d^{-1}. Shading is over 4, 8 and 16 mm d^{-1}. (c) Qsat − Ctrl difference (contours every 2 mm d^{-1}) and model topography (shading above 500, 1000 and 3000 m altitude).

The moisture and precipitation changes are also enhanced by a feedback on the mean winds differences. The diminution of latent heat release over the summits leads to less mass convergence and still less precipitation (not shown). The relative humidity decrease over the southern Andes is also due to the lack in Qsat of advection of moist air from the ocean forced by the heating over the mountains. This region, close to the Atacama desert, is indeed quite dry in the observations.

The changes in Q_{rel} over Asia (Fig. 5) are again consistent with those over South America: the main signature is an increase of relative humidity on the mountain slopes, observed in Ethiopia but above all around the Tibetan Plateau. The Indo-Gangetic plain in north-east India moistens considerably up to the Punjab region, which, together with the decrease of latent heating on the east side of the Himalayas, explains the shift of the monsoon precipitation core to the bay of Bengal.

4.3. Influence of resolution

This problem of advection of supersaturated air occurs mainly at a one grid-point scale, so it can be expected that the model resolution will influence the previous results. The relevant quantity to determine the error in the amount of advected water vapour is the temperature (or saturation mixing ratio) difference between two neighbouring points. Increased horizontal resolution acts both to decrease this difference by reducing the distance between grid points and to increase it by allowing generally higher mountains and so steeper temperature gradients. The net effect is thus not clear.

In their study of the effect of resolution on the simulation of the Indian monsoon, Stephenson et al. (1998) did a series of experiments with both a high-resolution (T63, HR hereafter) and a low-resolution (T21, LR) model. A third experiment, here called HR/LO, used the high T63 resolution but with the smoother and lower orography of

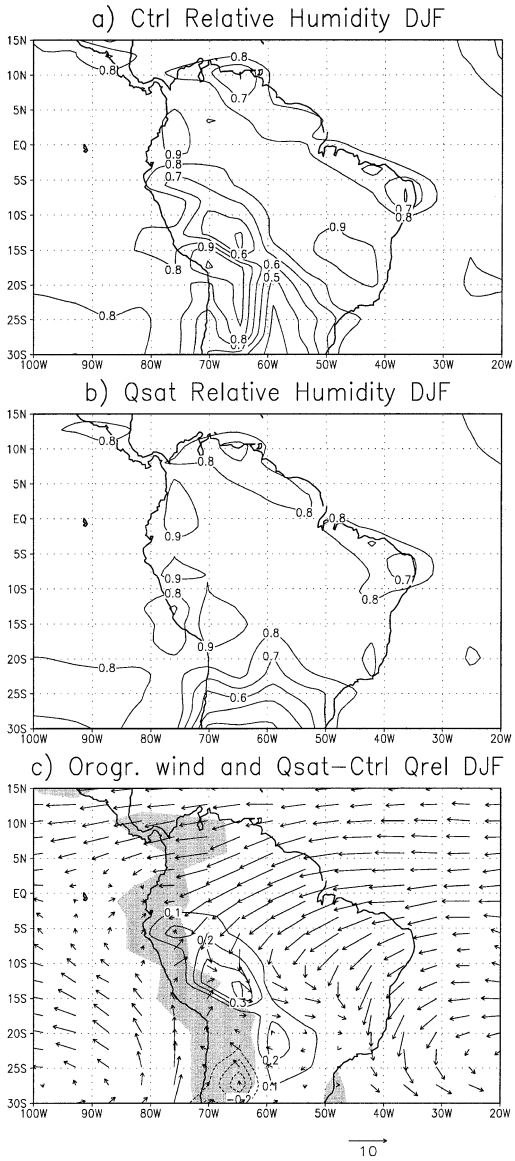

Fig. 4. December–January–February relative humidity at 5 m. (a) Ctrl run, (b) Qsat run and (c) Qsat − Ctrl difference (contour), mean 850 hPa winds and model orography (shaded, levels as Fig. 2).

the T21 model. They found that in the HR/LO model, the precipitation over the southern slopes of the Tibetan plateau was reduced compared to the HR experiment. This could have been expected, since they were using the same model with a lower relief. However, the precipitation in the HR/LO run was also reduced compared to the full LR run, which had the same orography but a lower resolution. This effect could perhaps be explained this way: with a higher resolution, the altitude difference between two adjacent points is lower even though the slope is the same. This minimises spurious water vapour advection and keeps rainfall amounts down.

To test this, we did another sensitivity experiment using a model with a 50% higher horizontal resolution, keeping the same two advection schemes as in the lower resolution experiments. The results for the Asian monsoon region are shown in Fig. 6.

As in the low-resolution case, the rainfall amount decreases over the Ethiopian mountains and the Tibetan Plateau, while it increases in a thin band over the southern Himalaya slopes. The location of this tongue of heavy precipitation coincides well with that seen in the observations of Legates and Willmott (1990). The intensity is, however, much too strong at several grid points. There is very strong convection over these points in both experiments, and the rainfall gets stronger in Qsat when little moisture is advected over Tibet. The location of these points also coincides with large pressure anomalies on the σ-surfaces.

A new feature in the high-resolution runs is the effect of the Western Ghats, which are now resolved. In the Ctrl run, the corresponding rainfall maximum is located over the mountain range, while in Qsat it is more to the west, leaving the eastern part of southern India drier. This is again in better agreement with the observations. The precipitation increase on the western coast of Burma is another improvement.

5. Discussion and conclusions

Even sophisticated water vapour advection schemes, which calculate elaborated approximations of the sub-grid humidity distribution, do not generally take into account the underlying temperature field. This can result in estimated values of the advected mixing ratio q which exceed local saturation. Along constant pressure levels, this effect will be relatively weak, as it will depend only on horizontal temperature gradients. However, it yields a systematic bias along constant low-level terrain-following coordinate surfaces,

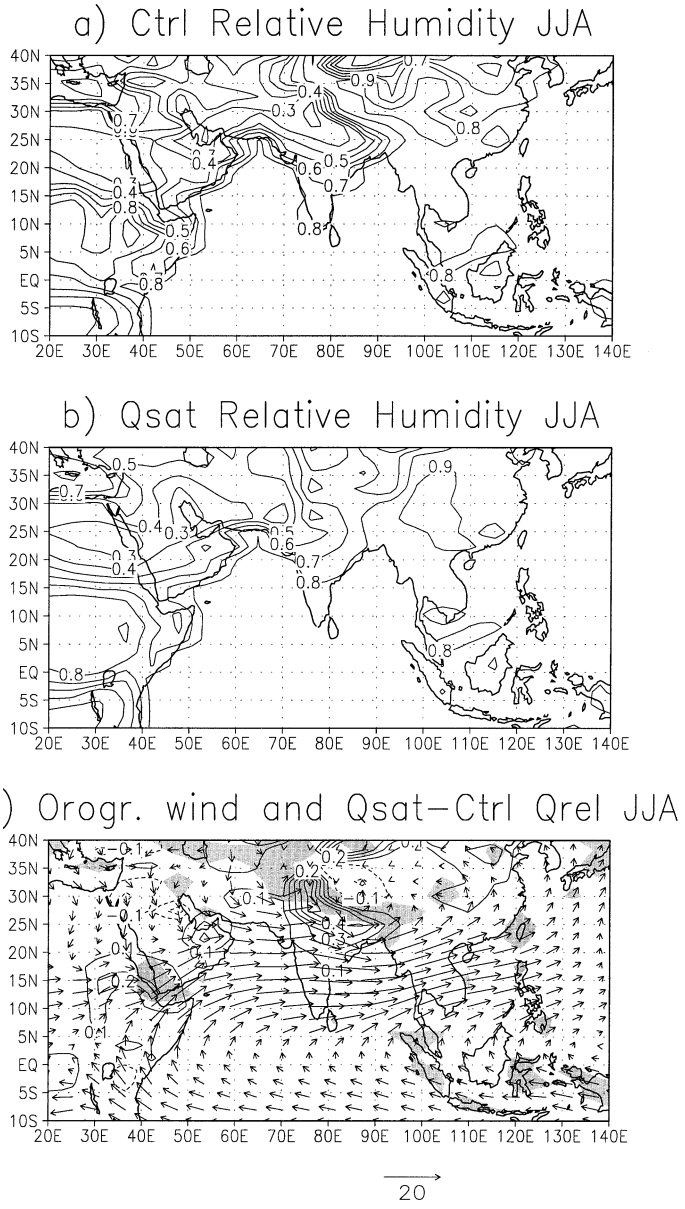

Fig. 5. June–July–August relative humidity at 5 m. (a) Ctrl run, (b) Qsat run and (c) Qsat − Ctrl difference (contours), mean 850 hPa winds and model orography (shaded, levels as Fig. 3).

where there is an upslope decrease of temperature. In that case, water is artificially advected in the vapour phase to mountain summits, where it eventually condenses, causing a spurious displacement of precipitation from foothills and slopes to summits. This error in rainfall location also feeds back on the spurious water vapour convergence over orography due to the errors in the horizontal pressure gradient in terrain-following coordinates. Note that the same problem theoretically exists with horizontal diffusion. However, we found that in our model, horizontal diffusion accounts for

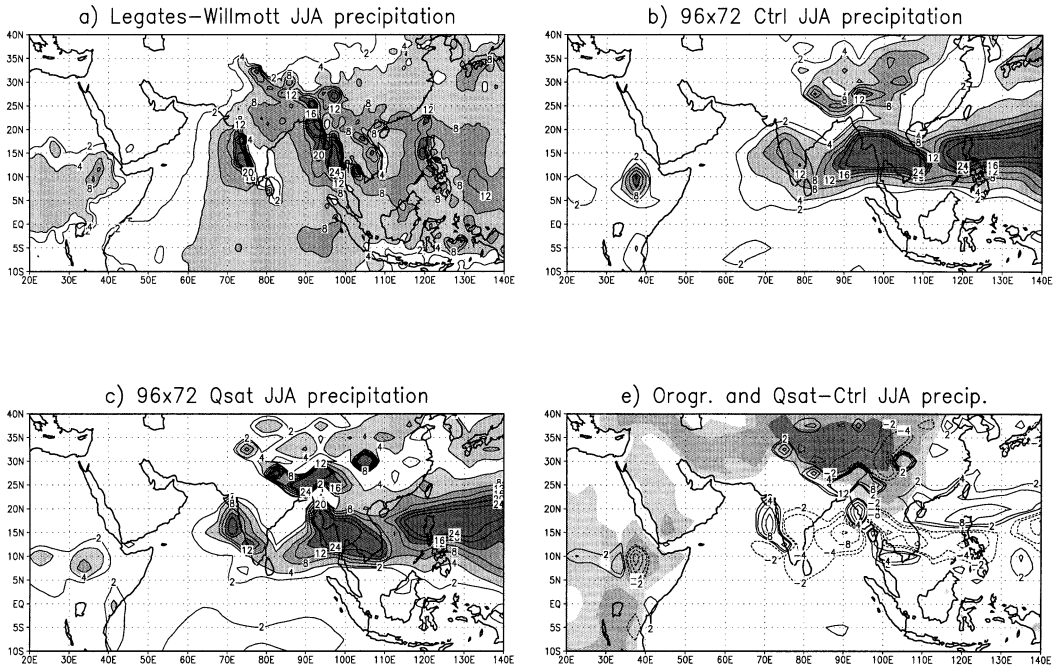

Fig. 6. June–July–August moonsoon precipitation (mm d^{-1}). (a) Observations, (b) high-resolution Ctrl and (c) Qsat runs. Contours are every 4 and at 2 mm d^{-1}. Shading is over 4, 8 and 16 mm d^{-1}. (e) Qsat − Ctrl difference (contours every 2 mm d^{-1}) and model topography (shaded, as in Fig. 3).

less than 10% of the evolution of water vapour due to atmospheric dynamics. The fact that by only modifying the advection scheme almost all the orographic maxima are removed also indicates that diffusion must play a minor role.

To suppress this rainfall bias, we propose to modify the horizontal advection scheme by limiting the amount of advected water vapour that reaches the downwind point, using the saturation mixing ratio, and by redistributing the excess water vapour along the path. This solution is physically based, and can be implemented in any finite difference advection scheme in flux form. Here we have tested this idea using a simple scheme, based on upstream finite differencing, where the excess water vapour is kept at the upstream point. This is a reasonable assumption, because of the exponential dependence of q_{sat} on temperature.

We tested the sensitivity of the precipitation simulated by the LMD GCM to this process by focusing on the Asian and Amazonian summer monsoons. The effect is particularly strong using an upstream advection scheme. In the absence of saturation limiters, the rainfall is concentrated in strong maxima situated over the mountains. The resulting latent heat release in turn causes air mass convergence which brings more moisture, and amplifies the phenomenon. Simultaneously, there is a subsidence and horizontal divergence in the adjacent valleys or foothills, resulting in low relative humidity and weak precipitation. Moisture is thus 'pumped up' to the summits.

When saturation limiters are added, the relative humidity remains high over the summits, but does not exceed saturation when there is no air mass convergence. Owing to the same feedback loop as above, orographic precipitation maxima then decrease strongly or move downslope. The water vapour which is not advected upward remains in the valleys and along the slopes, upstream of the mountains. Here moisture is 'trapped' downhill, as it should be because of the exponential decrease of water vapour mixing ratio with temperature.

The precipitation simulated with the modified schemes compares much better to the observations

of Legates and Willmott. The rainfall rates tend to be more evenly distributed, with less spurious maxima or dry areas, and the location of the extrema is better. A study of river run-off also displays an improvement, due to the decrease of precipitation over land (J. L. Dufresne, personal communication).

The improvements are still significant using a higher horizontal resolution. Even though the changes in the location of the precipitation maxima are on a smaller spatial scale, the simulation at a given resolution is still improved.

However small the extent of these rainfall shifts, they can also have a strong influence on the regional, or even global simulated climate. Heavy rainfall feeds back on larger-scale atmospheric circulation through the effects of both latent heat release and cloud radiative forcing. Indeed, it was found that strong winds over the south-eastern Pacific driven by spurious latent heating over the Andes had a strong negative effect on a coupled atmosphere–ocean model (Codron et al., 2001; Codron, 2001). Both the mean state and variability greatly improved upon introducing the new advection scheme.

The simulated rainfall is still far from perfect: rainfall rates can reach unrealistic high values in some well defined areas, whereas other regions such as the Amazon basin or central and eastern India appear too dry, particularly in the high-resolution experiments. These discrepancies may be partly attributed to the erroneous pressure gradient near orography, and are reinforced by the general tendency of the model to produce spatially concentrated rainfall. The reasons are not clear, but almost certainly involve the convection scheme.

The simple physical constraint we proposed should help reducing biases in the rainfall pattern related to orography, and their more global reflections. With less diffusive advection schemes and hybrid coordinates (giving fewer pressure gradient errors), we expect that the precipitation bias due to water vapour advection will be less. The impact of our modification should, however, still remain positive. The computational cost added is moderate, and the method can be generalised to other types of schemes like the semi-Lagrangian one.

6. Acknowledgments

This publication is supported by a grant to the Joint Institute for the Study of the Atmosphere and Ocean (JISAO) under NOAA Cooperative Agreement No. NA17RS1232. The numerical experiments have been conducted at IDRIS (Institut de Développement et de Recherches en Informatique Scientifique) of the Centre National de la Recherche Scientifique.

REFERENCES

Codron, F. 2001. Sensitivity of the tropical Pacific to a change of orbital forcing in two versions of a coupled GCM. *Climate Dynam.* **17**, 205–212.

Codron, F., Vintzileos, A. and Sadourny, R. 2001. Influence of mean state changes on the structure of ENSO in a tropical coupled GCM. *J. Climate* **14**, 730–742.

Fouquart, Y. and Bonnel, B. 1980. Computation of solar heating of the earth's atmosphere: a new parametrization. *Beitr. Phys. Atmos.* **53**, 35–62.

Harzallah, A. and Sadourny, R. 1995. Internal versus SST-forced atmospheric variability as simulated by an atmospheric general circulation model. *J. Climate* **8**, 474–495.

Kuo, H. 1965. On formation and intensification of tropical cyclones through latent heat release by cumulus convection. *J. Atmos. Sci.* **22**, 40–63.

Le Treut, H. and Li, Z.-X. 1991. Sensitivity of an atmospheric general circulation model to prescribed SST changes: feedback effects associated with the simulation of cloud optical properties. *Climate Dynam.* **5**, 175–187.

Legates, D. R. and Willmott, C. J. 1990. Mean seasonal and spatial variability in gauge-corrected, global precipitation. *Intl. J. Climatol.* **10**, 111–127.

Manabe, S. and Strickler, R. 1964. Thermal equilibrium of the atmosphere with a convective adjustment. *J. Atmos. Sci.* **21**, 361–385.

Morcrette, J. J. 1991. Radiation and cloud radiative properties in the ECMWF operational weather forecast model. *J. Geophys. Res.* **96**, 9121–9132.

Nanjundiah, R. S. 2000. Impact of the moisture transport formulation on the simulated tropical rainfall in a general circulation model. *Climate Dynam.* **16**, 303–317.

Phillips, N. A. 1957. A coordinate system having some special advantages for numerical forecasting. *J. Meteorol.* **14**, 184–185.

Prather, M. J. 1986. Numerical advection by conserva-

tion of second order moments. *J. Geophys. Res.* **91**, 6671–6681.

Rasch, P. J. and Williamson, D. L. 1991. The sensitivity of a general circulation model to moisture transport formulation. *J. Geophys. Res.* **96**, 13,123–13,137.

Sadourny, R. 1975. The dynamics of finite-difference models of the shallow-water equations. *J. Atmos. Sci.* **32**, 680–689.

Simmons, A. and Burridge, D. 1981. An energy and angular momentum conserving vertical finite difference scheme in hybrid vertical coordinate. *Mon. Weather. Rev.* **106**, 758–766.

Stephenson, D. B., Chauvin, F. and Royer, J. F. 1998. Simulation of the Asian summer monsoon and its dependence on model horizontal resolution. *J. Meteorol. Soc. Jpn.* **76**, 236–265.

Van Leer, B. 1977. Towards the ultimate conservative difference scheme: IV. A new approach to numerical convection. *J. Comput. Phys.* **23**, 276–299.

Vintzileos, A., Delecluse, P. and Sadourny, R. 1999a. On the mechanisms in a tropical ocean–global atmosphere general circulation model. Part I: Mean state and the seasonal cycle. *Climate Dynam.* **15**, 43–62.

Vintzileos, A., Delecluse, P. and Sadourny, R. 1999b. On the mechanisms in a tropical ocean–global atmosphere general circulation model. Part II: Interannual variability and its relation to the seasonal cycle. *Climate Dynam.* **15**, 63–80.

Webb, M., Senior, C., Bony, S. and Morcrette, J.-J. 2001. Combining ERBE and ISCCP data to assess clouds in the Hadley Center, ECMWF and LMD atmospheric climate models. *Climate Dynam.* **17**, 905–922.

Williamson, D. L. and Rasch, P. J. 1994. Water vapor transport in the NCAR CCM2. *Tellus* **46A**, 34–51.

Zhu, Z. 1997. Precipitation and water vapor transport simulated by a hybrid $\sigma - \theta$ coordinate GCM. *J. Climate* **10**, 988–1003.